Rotating tensiometer for the measurement of the elastic modulus of deformable particles

Massimiliano M. Villone*
Dipartimento di Ingegneria Chimica, dei Materiali e della Produzione Industriale, Università di Napoli Federico II, P. le Tecchio 80, 80125 Napoli, Italy

Howard A. Stone
Department of Mechanical and Aerospace Engineering, Princeton University, Princeton, New Jersey 08544, U.S.A.

(Received 15 May 2020; accepted 30 July 2020; published 19 August 2020)

In a spinning drop tensiometer, the interfacial tension between two immiscible fluids can be inferred from the equilibrium shape of a drop suspended in a denser rotating immiscible liquid [B. Vonnegut, Rev. Sci. Instrum. **13**, 6 (1942)]. For small deformations of the droplet, an analytical solution for the droplet's shape exists [H. A. Stone and J. W. M. Bush, Q. Appl. Math. **54**, 551 (1996)]. Similarly, we derive an analytical solution for the deformation dynamics of an initially spherical elastic particle suspended in a denser viscous rotating liquid. At long times, the particle attains a steady-state deformed shape that depends on the rotational Bond number, from which it is possible to get a measurement of the particle's elastic modulus, thus giving a proof of concept for a rotating tensiometer. Direct numerical simulations are used to validate the theory and identify its limits of applicability.

DOI: 10.1103/PhysRevFluids.5.083606

I. INTRODUCTION

Suspensions of deformable solid particles in a liquid are frequent in both nature and applications. Consider, for example, filled polymers [1], suspensions of microgel beads or starch granules [2], and biological fluids carrying cells [3]. Being able to measure the mechanical properties of deformable particles is important for understanding and controlling the behavior of the aforementioned suspensions. Furthermore, some biological particles show different deformability depending on whether they are healthy or diseased [4,5], so measuring their mechanical properties can be a powerful tool to evaluate their health.

In the last two decades, several methods for measurement of the mechanical properties of submillimetric deformable particles have appeared in the literature. Some examples are atomic-force-microscopy-based techniques [6,7], micropipette aspiration [8], compression between parallel plates [9–12], osmotic compression [13–17], and capillary micromechanics [18–20]. Very recently, microfluidic approaches have proved to be suitable for the measurement of particle elasticity in continuous flow [21–24]. An overview of the available techniques for the measurement of the mechanical properties of deformable solid particles can be found in Ref. [25].

The measurement of the deformability of very soft particles, e.g., microgel beads with a low elastic modulus, can be very difficult when the 'traditional' techniques based on contact, e.g., nanoindentation, are used [24]. In a spinning drop tensiometer, the interfacial tension between two immiscible fluids can be inferred from the equilibrium shape of a drop suspended in a denser

*massimiliano.villone@unina.it

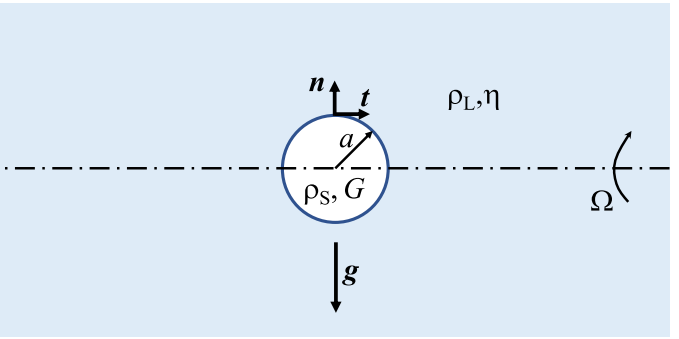

FIG. 1. Schematic of an initially spherical elastic particle suspended on the axis of a rotating viscous liquid.

rotating immiscible liquid [26]. Similarly, in this paper we propose to infer the elastic modulus of a soft particle from its equilibrium deformed shape, thus giving a proof of concept for a rotating tensiometer. To do this, we present an exact solution of the deformation of an initially spherical elastic particle suspended on the axis of a denser viscous rotating liquid. Direct numerical simulations are used to validate the theory and to identify its limits of applicability.

II. MATHEMATICAL MODEL AND ANALYTICAL SOLUTION OF THE PROBLEM

Let us consider an unbounded Newtonian liquid with density ρ_L and viscosity η rotating at constant angular frequency Ω around the horizontal axis. An initially spherical elastic particle with radius a, density ρ_S, and shear elastic modulus G is placed with its center on the rotation axis of the fluid (see Fig. 1). Provided $\Delta\rho = \rho_L - \rho_S > 0$, the center of mass of the particle is stable along the axis. We assume that (i) both the phases are incompressible—for the solid material, this means that the Poisson ratio $\nu = 1/2$, which is a good approximation for many deformable materials, e.g., hydrogels [27]; (ii) the centrifugal pressure field dominates the gravitational pressure field, thus gravitational effects can be neglected, i.e., $g/a\Omega^2 \ll 1$, with g the magnitude of the gravitational acceleration; (iii) Coriolis forces are negligible with respect to viscous forces, i.e., the Taylor number $\mathrm{Ta} = \Omega a^2\rho/\eta$ is much smaller than unity; and (iv) inertial effects are negligible, i.e., the Reynolds number $\mathrm{Re} = \Delta\rho\Omega^2 a^4\rho/\eta^2$ is much smaller than unity, where the characteristic velocity $u = \Delta\rho\Omega^2 a^3/\eta$ arises from balancing the characteristic centrifugal pressure $\Delta\rho\Omega^2 a^2$ and the characteristic viscous stress $\eta u/a$. Under these assumptions, the system is modeled through the mass and momentum balance equations on the liquid and the solid domains in the Stokes regime, which are

$$\nabla \cdot \boldsymbol{u} = 0, \tag{1a}$$

$$\nabla \cdot \boldsymbol{T} = \boldsymbol{0}, \tag{1b}$$

where $\boldsymbol{u}$ is the velocity vector and $\boldsymbol{T}$ is the stress tensor. For both phases, the stress tensor is $\boldsymbol{T} = -p_d\boldsymbol{I} + \boldsymbol{\sigma}$, with p_d the dynamic pressure and $\boldsymbol{\sigma}$ the deviatoric part of the stress tensor, for which a constitutive equation has to be chosen. In the liquid, the Newtonian constitutive equation is chosen, reading

$$\boldsymbol{\sigma} = 2\eta\boldsymbol{D}, \tag{2}$$

with $\boldsymbol{D} = (\nabla\boldsymbol{u} + \nabla\boldsymbol{u}^{\mathrm{T}})/2$ the symmetric part of the velocity gradient tensor $\nabla\boldsymbol{u}$, whereas in the solid, we consider Hooke's law,

$$\boldsymbol{\sigma} = G\boldsymbol{B}, \tag{3}$$

with $\boldsymbol{B}$ the left Cauchy-Green deformation tensor (or Finger tensor, dimensionless). The dynamic pressure p_d is defined as the sum of the actual pressure p and the centrifugal pressure $(1/2)\rho(\boldsymbol{\Omega}\times\boldsymbol{r})^2$, where $\boldsymbol{r}$ denotes the position vector from the rotation axis, i.e., $p_\mathrm{d} = p + (1/2)\rho(\boldsymbol{\Omega}\times\boldsymbol{r})^2$.

The balance equations reported above are supplied with boundary conditions on the interface between the particle and the ambient fluid:

$$\boldsymbol{u}|_\mathrm{L} = \boldsymbol{u}|_\mathrm{S}, \tag{4a}$$

$$\boldsymbol{t}\cdot(\boldsymbol{n}\cdot\boldsymbol{T}|_\mathrm{L}) = \boldsymbol{t}\cdot(\boldsymbol{n}\cdot\boldsymbol{T}|_\mathrm{S}), \tag{4b}$$

$$\boldsymbol{n}\cdot(\boldsymbol{n}\cdot\boldsymbol{T}|_\mathrm{L}) = \boldsymbol{n}\cdot(\boldsymbol{n}\cdot\boldsymbol{T}|_\mathrm{S}) + \tfrac{1}{2}\Delta\rho(\boldsymbol{\Omega}\times\boldsymbol{r})^2. \tag{4c}$$

Equations (4), with the subscript 'L' denoting the liquid, 'S' denoting the solid, $\boldsymbol{t}$ the unit vector tangent to the solid-liquid interface, and $\boldsymbol{n}$ the unit vector normal to the solid-liquid interface and directed towards the liquid, express the velocity and stress continuity across the aforementioned interface, respectively. In this regard, we have assumed that solid surface tension is negligible with respect to elasticity, this assumption being justified below.

We make the governing equations dimensionless by choosing a as the characteristic length, $u = \Delta\rho\Omega^2 a^3/\eta$ as the characteristic velocity, $\eta u/a$ as the characteristic pressure in the fluid, and G as the characteristic pressure in the solid. The dimensionless versions of Eqs. (1) and (4a) are formally the same as the dimensional ones, whereas the dimensionless expressions of Eqs. (4b) and (4c) are

$$\mathrm{Bo}\,\boldsymbol{t}^*\cdot(\boldsymbol{n}^*\cdot\boldsymbol{T}^*|_\mathrm{L}) = \boldsymbol{t}^*\cdot(\boldsymbol{n}^*\cdot\boldsymbol{T}^*|_\mathrm{S}), \tag{5a}$$

$$\mathrm{Bo}\,\boldsymbol{n}^*\cdot(\boldsymbol{n}^*\cdot\boldsymbol{T}^*|_\mathrm{L}) = \boldsymbol{n}^*\cdot(\boldsymbol{n}^*\cdot\boldsymbol{T}^*|_\mathrm{S}) + \frac{\mathrm{Bo}}{2}(\boldsymbol{\Omega}^*\times\boldsymbol{r}^*)^2, \tag{5b}$$

with superscript asterisks denoting dimensionless quantities and $\mathrm{Bo} = \Delta\rho\Omega^2 a^2/G$ the rotational Bond number measuring the relative magnitude of centrifugal stresses causing particle deformation and elastic stresses resisting it.

The centrifugal force makes the particle deform. For small values of the Bond number, i.e., $\mathrm{Bo} \ll 1$, the deformed shape of the particle is a prolate spheroid aligned with the rotation axis of the fluid and it can be determined analytically by following the procedures outlined by Murata for a linear elastic particle in an arbitrary flow field of a suspending liquid [28] and by Stone and Bush for a liquid droplet in a rotating ambient liquid [29]. Some mathematical details are given in the Appendix. The equations for the transient evolution of the major semiaxis L and the minor semiaxis B of the spheroid read

$$\frac{L}{a} = 1 - 2\alpha\mathrm{Bo}\left[\exp\left(-\frac{t}{t_r}\right) - 1\right], \tag{6a}$$

$$\frac{B}{a} = 1 + \alpha\mathrm{Bo}\left[\exp\left(-\frac{t}{t_r}\right) - 1\right], \tag{6b}$$

with $\alpha = 16/5$ and the relaxation time $t_r = (15/8)\eta/G$. Equations (6) are formally the same as those for a liquid droplet [29], yet in that case $\alpha = 1/24$ and $t_r = ((3+2\lambda)(16+19\lambda)/(40(1+\lambda))\eta a/\gamma$, with λ the viscosity ratio of the droplet to the matrix liquid and γ the surface tension between the two liquids (and of course the definition of the Bond number is different).

At long times, namely, when $t \to \infty$, the particle tends to attain a steady-state deformed shape. The latter can be synthetically expressed through the Taylor deformation parameter $D = (L-B)/(L+B)|_{t\to\infty}$. In terms of D, the steady-state deformed shape of the particle is

$$D = \frac{3\alpha\mathrm{Bo}}{2+\alpha\mathrm{Bo}}, \tag{7}$$

which is independent of the viscosity of the fluid since the final steady state is a rigid-body motion.

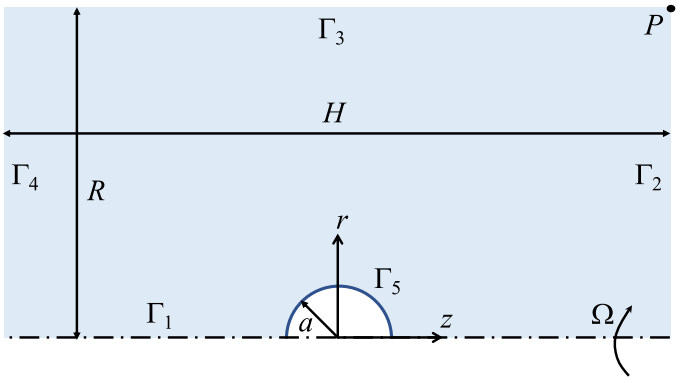

FIG. 2. Schematic of the computational domain for finite-element numerical simulations. (Not to scale).

III. DIRECT NUMERICAL SOLUTION OF THE PROBLEM AND COMPARISON BETWEEN THE SOLUTIONS

In order to validate the analytical solutions expressed by Eqs. (6) and (7) and to investigate their limits of applicability, we perform direct numerical simulations with the finite-element method. Due to the geometry of the system, we consider the two-dimensional axisymmetric computational domain depicted (not to scale) in Fig. 2. A cylindrical coordinate system is set with its origin in the center of the particle. It is worth remarking that, at variance with the theoretical situation, where the particle is rigorously unbounded, the domain for numerical simulations has finite length H and radius R, yet it is verified that these dimensions are sufficiently larger than the dimension of the particle so as to ensure that for practical purposes the latter can be considered unbounded.

The mathematical model is constituted by the mass and momentum balance equations on both the liquid and the solid phase given by Eqs. (1). For the liquid, we use the Newtonian constitutive equation. For the elastic particle, since we aim at simulating also cases in which Bo is nonvanishing, we choose the neo-Hookean constitutive equation, which predicts the same behavior as the Hookean form at small deformation but is more realistic at finite deformation. Its velocity-based formulation is [30]

$$\overset{\triangledown}{\boldsymbol{\sigma}} = 2G\boldsymbol{D}, \tag{8}$$

with the symbol $\triangledown$ indicating the upper convected time derivative.

The mass and momentum balance equations are supplied with the axial symmetry condition on the boundary Γ_1, the unperturbed rotational velocity profile of the fluid $u(r, \theta, z) = (0, \Omega r, 0)$ on Γ_2–Γ_4, and the continuity of velocity and stress between the solid and the liquid on Γ_5 [see Eqs. (4)]. Furthermore, a reference pressure value equal to 0 is set at point P.

Since both the particle and the suspending medium are inertialess, no initial condition on the velocity is required, whereas an initial condition is needed for the tensor $\boldsymbol{\sigma}$ in the elastic phase. We assume that the particle is initially stress-free, namely,

$$\boldsymbol{\sigma}|_{t=0} = \mathbf{0}. \tag{9}$$

The equations governing the system are solved through the arbitrary Lagrangian-Eulerian finite-element method. The details on our numerical technique for the simulation of the behavior of suspensions with deformable inclusions can be found in Ref. [31].

Both the liquid and the solid domains are discretized by means of a computational grid (mesh) made of quadratic triangles. The elements at the interface between the two phases are the same on both the matrix and the particle side (conforming geometry). Figure 3 shows a view of the portion of the mesh in the proximity of the particle. During the simulations, the elements of the mesh can

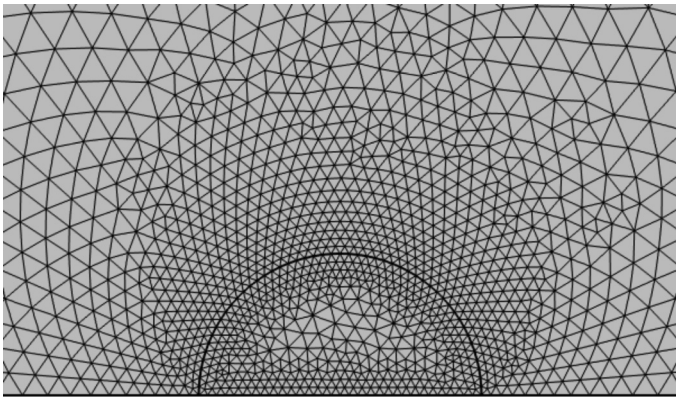

FIG. 3. View of the portion of the mesh in the proximity of the particle.

distort because of particle deformation. Anytime the quality of the elements of the mesh anywhere in the domain becomes unacceptable in terms of a threshold (which is likely to occur at 'high' Bo values), a remeshing is performed, and the solution is projected from the old mesh to the new one as technically detailed in Ref. [32].

Before running simulations, convergence tests are performed in space and time, i.e., the mesh resolution and time step for the numerical solution of the equations presented above are chosen so as to ensure invariance of the results upon further refinements.

We run finite-element numerical simulations at increasing Bo up to 0.15, from which we track 'real time' the deformation of the particle until it attains a steady-state shape. In Fig. 4, we display the time evolution of the major and minor semiaxes of the prolate spheroid corresponding to the deformation of a particle at Bo $= 0.003$. The dashed lines report the theoretical predictions arising from Eqs. (6), whereas the circles represent the results from direct numerical simulations. It is apparent that, for a small Bo, there is quantitative agreement between the analytical and the numerical solution.

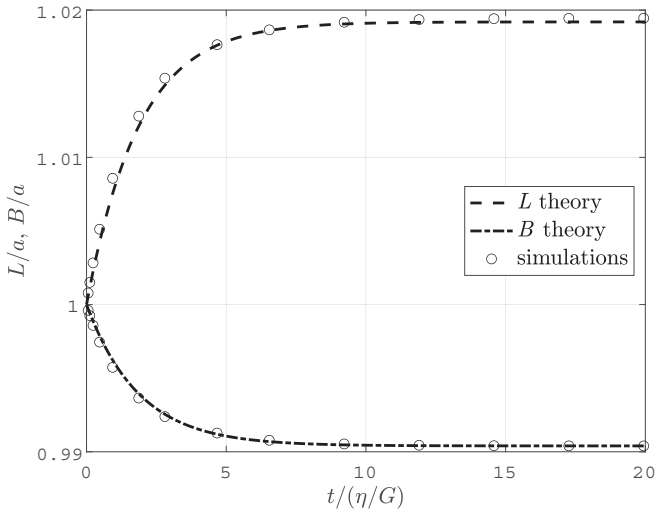

FIG. 4. Time evolution of the major and minor semiaxes of the prolate spheroid corresponding to the deformation of a particle at Bo $= 0.003$.

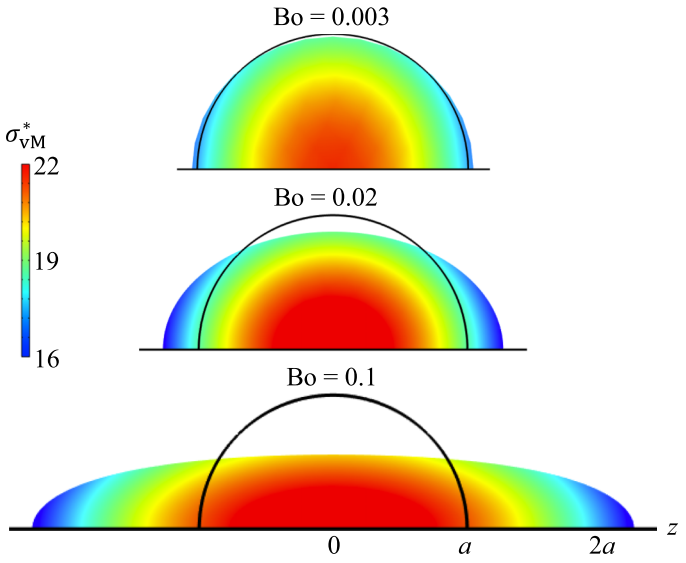

FIG. 5. Steady-state deformed shape of the particle at three increasing orders of magnitude of Bo with color maps of the dimensionless von Mises stress σ^*_{vM} in the longitudinal section of the particle.

In Fig. 5, we show the steady-state deformed shape of the particle at three different orders of magnitude of Bo. In particular, going from top to bottom, Bo = 0.003, 0.02, and 0.1 are considered. For each image, the trace of the undeformed initial shape of the particle is also reported, from which the progressively more pronounced departure from sphericity of its steady-state distorted shape can be readily appreciated. The color maps give the distribution of the dimensionless von Mises stress $\sigma^*_{vM} = \sqrt{(3/2)\boldsymbol{\sigma} : \boldsymbol{\sigma}}/(\Delta\rho\Omega^2 a^2)$ in the longitudinal section of the particle, which is a scalar measure of its stress state [33]. It is apparent that the stress distribution in the axial direction is qualitatively similar at every Bo, whereas this is not true in the radial direction. From the quantitative point of view, the explored stress range scales with the rotational stress $\Delta\rho\Omega^2 a^2$; indeed, all the maps have the same color scale.

Finally, we display in Fig. 6 the analytical prediction, Eq. (7), for the steady-state value of the Taylor deformation parameter D as a function of Bo (dashed line) and the numerical values arising from finite-element simulations at varying Bo (circles). It is apparent that for Bo $\lesssim 0.02$ there is quantitative agreement between the analytical and the numerical solutions, which is lost for larger Bo, with the theory increasingly overestimating D with respect to the numerical simulations at increasing Bo. The appearance of a discrepancy is of course expected since the theoretical solution considers a small departure of the shape of the particle from sphericity and is derived in the limit of Bo $\ll 1$. Nevertheless, the results of finite-element simulations show that the theoretical predictions are quantitatively reliable even for finite values of the deformation (the D value at Bo $= 0.02$ is almost equal to 0.1).

The results presented in this paper represent a proof of concept for the possibility of using a simple and commercially available device, i.e., the spinning drop tensiometer, for measurement of the elastic modulus of deformable beads based on their distortion in a rotating viscous fluid. Indeed, if a particle with initial radius a and density ρ_S is suspended on the axis of a flow cell containing a liquid with density $\rho_L > \rho_S$ and viscosity η that is rotating at angular frequency Ω, the optical measurement of the steady-state value of the deformation parameter of the particle D (provided it is within about 0.1) will allow determination of the corresponding Bo through the solution of Eq. (7) and, thus, of the value of the shear elastic modulus of the particle G. In particular, this method could be useful in measuring the elastic properties of soft gel particles, for which the more 'traditional' and

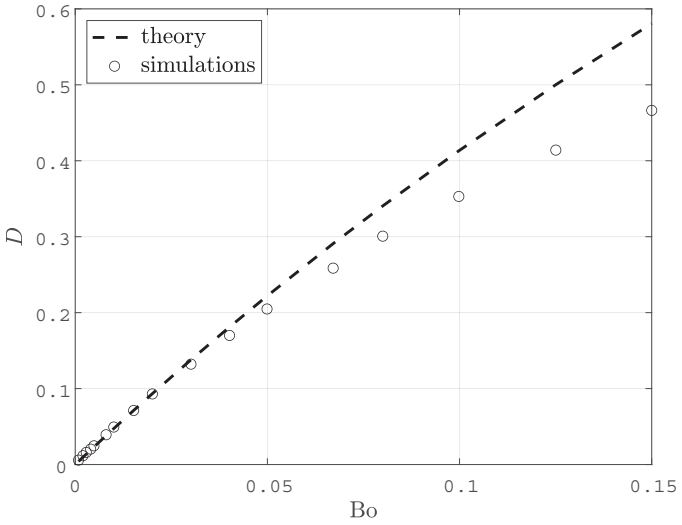

FIG. 6. Steady-state values of the 'Taylor' deformation parameter D as a function of the Bo arising from Eq. (7) (dashed line) and from finite-element numerical simulations (circles).

'invasive' techniques, e.g., nanoindentation, are likely to fail due to the particle's great deformability [24]. As an example, let us consider a gel microparticle with radius $a = 500\,\mu$m, density $\rho_S = 970\,\mathrm{kg\,m^{-3}}$, and elastic modulus $G = 1\,$kPa suspended in a fluid with density $\rho_L = 1000\,\mathrm{kg\,m^{-3}}$ and viscosity $\eta = 100\,$pa s rotating at angular frequency $\Omega = 1500\,\mathrm{s^{-1}}$. (The values of η and Ω have been chosen by referring to the literature on spinning drop tensiometry for measurement of the interfacial tension between liquids [34].) Under those conditions, we would obtain a Bo value of about 0.02. At the same time, $g/(a\Omega^2)$ and Ta are $O(10^{-3})$ and $\mathrm{Re} = O(10^{-7})$, thus confirming their smallness in the system. For smaller particles, comparable values of Bo could by achieved by increasing Ω slightly, which is still practically feasible in commercially available rotating devices [34]. Finally, we verify that solid surface tension can be neglected by evaluating $\gamma_{sv}/(Ea)$ [35], with γ_{sv} the surface tension coefficient of the deformable particle, E its Young modulus (equal to $3G$ due to incompressibility), and a its characteristic dimension. By taking $\gamma_{sv} = 0.03\,\mathrm{N\,m^{-1}}$ [36], $E = 3 \times 10^3\,$kPa, and $a = 500 \times 10^{-6}\,$m, we obtain $\gamma_{sv}/(Ea) = 0.02 \ll 1$, thus confirming the validity of the assumption of neglecting solid surface tension with respect to elasticity.

IV. CONCLUSIONS

In this paper, we present an analytical solution for the transient deformation of an initially spherical elastic particle suspended in a denser viscous rotating liquid. A close analogy is found with the solution for a liquid droplet in an immiscible ambient liquid under the same conditions [29]. At long times, the deformation of the particle attains a steady-state value that depends on the rotational Bond number $\mathrm{Bo} = \Delta\rho\Omega^2 a^2/G$, with $\Delta\rho$ the density difference between the two phases, Ω the rotational angular frequency, a the particle radius, and G its shear elastic modulus. Therefore, given all the other parameters, the steady-state deformed shape of the particle allows us to infer its elastic modulus, thus giving a proof of concept for a rotating tensiometer. Finite-element numerical simulations are used to validate the theory and to identify its limits of applicability, which turn out to be $\mathrm{Bo} \simeq 0.02$. In addition, it is worth mentioning that the very first experimental results proving the actual usability of the rotating tensiometer for the measurement of the elastic modulus (and possibly the surface tension) of soft beads have appeared very recently in the literature [37].

APPENDIX

According to Murata [28], the equilibrium deformed shape of an initially spherical linear elastic particle of radius a suspended in an arbitrary flow field of a Newtonian fluid can be expressed in spherical coordinates as

$$\frac{r}{a} = 1 + \varepsilon f^{(1)}(\theta, \phi) + O(\varepsilon^2), \tag{A1}$$

with the dimensionless parameter $\varepsilon \ll 1$ representing the ratio of forces causing a particle's distortion to forces resisting it. Thus, in our case, $\varepsilon = \mathrm{Bo}$.

The product $\varepsilon f^{(1)}$ can be written in terms of the harmonic functions θ^* and χ^* (see Eq. (5.2) in Ref. [28]) as

$$\varepsilon f^{(1)} = \tau \frac{5}{114} \frac{1}{r^2} (114\phi^* + 9a^2\chi^*), \tag{A2}$$

with τ a 'constitutive' time and the harmonic functions containing the flow characteristic time. Thus, in our case, $\tau = \Delta\rho\Omega a^2/G$.

If the undisturbed flow field is expressed by means of the harmonic function

$$\phi^* = \frac{32}{25}\Omega r^2 \cos\left(\frac{4}{3}\theta\right), \tag{A3}$$

the steady-state deformed shape of the particle finally reads

$$\frac{r}{a} = 1 + \frac{32}{5}\mathrm{Bo}\cos\left(\frac{4}{3}\theta\right), \tag{A4}$$

which is the equation of a prolate spheroid, whose major semiaxis is obtained for $\theta = 0$, being equal to $L/a = 1 + (32/5)\mathrm{Bo}$, and whose minor semiaxis is obtained for $\theta = \pi/2$, being equal to $B/a = 1 - (16/5)\mathrm{Bo}$.

At this point, since the deformation of an elastic particle in an arbitrary flow field of a liquid is similar to the deformation of a liquid droplet [28], the transient evolution of the spheroid's semiaxes is obtained by mapping the problem of a particle in a rotating fluid on that of a particle in uniaxial extensional flow as done for a liquid droplet by Stone and Bush [29], who find that in the two cases the droplet attains its equilibrium spheroidal shape with the same relaxation time, $((3 + 2\lambda)(16 + 19\lambda)/(40(1 + \lambda))\eta a/\gamma$. For this reason, we infer that also an elastic particle in a rotating fluid reaches its steady-state shape with the same relaxation time as in uniaxial extensional flow, i.e., $(15/8)\eta/G$ [24,38], finally obtaining Eqs. (6).

[1] I. Galaev and B. Mattiasson, *Smart Polymers: Applications in Biotechnology and Biomedicine* (CRC Press, Boca Raton, FL, 2007).

[2] M. Desse, D. Fraiseau, J. Mitchell, and T. Budtova, Individual swollen starch granules under mechanical stress: Evidence for deformation and volume loss, Soft Matter **6**, 363 (2010).

[3] M. King and D. Gee, *Multiscale Modeling of Particle Interactions: Applications in Biology and Nanotechnology* (John Wiley & Sons, New York, 2010).

[4] H. W. Hou, Q. S. Li, G. Y. H. Lee, A. P. Kumar, C. N. Ong, and C. T. Lim, Deformability study of breast cancer cells using microfluidics, Biomed. Microdev. **11**, 557 (2009).

[5] M. Fraldi, A. Cugno, L. Deseri, K. Dayal, and N. M. Pugno, A frequency-based hypothesis for mechanically targeting and selectively attacking cancer cells, J. R. Soc., Interface **12**, 20150656 (2015).

[6] V. V. Tsukruk and S. Singamaneni, *Scanning Probe Microscopy of Soft Matter: Fundamentals and Practices* (John Wiley & Sons, New York, 2012).

[7] A. Kumachev, E. Tumarkin, G. C. Walker, and E. Kumacheva, Characterization of the mechanical properties of microgels acting as cellular microenvironments, Soft Matter **9**, 2959 (2013).

[8] F. Guilak, J. R. Tedrow, and R. Burgkart, Viscoelastic properties of the cell nucleus, Biochem. Biophys. Res. Commun. **269**, 781 (2000).
[9] O. Thoumine, A. Ott, O. Cardoso, and J.-J. Meister, Microplates: A new tool for manipulation and mechanical perturbation of individual cells, J. Biochem. Biophys. Methods **39**, 47 (1999).
[10] E. A. G. Peeters, C. V. C. Bouten, C. W. J. Oomens, and F. P. T. Baaijens, Monitoring the biomechanical response of individual cells under compression: A new compression device, Med. Biol. Eng. Computi. **41**, 498 (2003).
[11] E. A. Peeters, C. W. Oomens, C. V. Bouten, D. L. Bader, and F. P. Baaijens, Viscoelastic properties of single attached c2c12 myoblasts, J. Biomech. Eng. **127**, 237 (2005).
[12] M. Yuan, X. Ju, R. Xie, W. Wang, and L. Chu, Micromechanical properties of poly (*n*-isopropylacrylamide) hydrogel microspheres determined using a simple method, Particuology **19**, 164 (2015).
[13] B. R. Saunders and B. Vincent, Microgel particles as model colloids: Theory, properties and applications, Adv. Colloid Interface Sci. **80**, 1 (1999).
[14] A. Fernandez-Nieves, A. Fernandez-Barbero, B. Vincent, and F. J. De las Nieves, Osmotic de-swelling of ionic microgel particles, J. Chem. Phys. **119**, 10383 (2003).
[15] M. Bradley, J. Ramos, and B. Vincent, Equilibrium and kinetic aspects of the uptake of poly (ethylene oxide) by copolymer microgel particles of *n*-isopropylacrylamide and acrylic acid, Langmuir **21**, 1209 (2005).
[16] A. F. Routh, A. Fernandez-Nieves, M. Bradley, and B. Vincent, Effect of added free polymer on the swelling of neutral microgel particles: A thermodynamic approach, J. Phys. Chem. B **110**, 12721 (2006).
[17] B. Sierra-Martin, J. A. Frederick, Y. Laporte, G. Markou, J. J. Lietor-Santos, and A. Fernandez-Nieves, Determination of the bulk modulus of microgel particles, Colloid Polym. Sci. **289**, 721 (2011).
[18] H. M. Wyss, T. Franke, E. Mele, and D. A. Weitz, Capillary micromechanics: Measuring the elasticity of microscopic soft objects, Soft Matter **6**, 4550 (2010).
[19] M. Guo and H. M. Wyss, Micromechanics of soft particles, Macromol. Mater. Eng. **296**, 223 (2011).
[20] T. Kong, L. Wang, H. M. Wyss, and Ho Cheung Shum, Capillary micromechanics for core–shell particles, Soft Matter **10**, 3271 (2014).
[21] A. Mietke, O. Otto, S. Girardo, P. Rosendahl, A. Taubenberger, S. Golfier, E. Ulbricht, S. Aland, J. Guck, and E. Fischer-Friedrich, Extracting cell stiffness from real-time deformability cytometry: Theory and experiment, Biophys. J. **109**, 2023 (2015).
[22] M. Mokbel, D. Mokbel, A. Mietke, N. Traber, S. Girardo, O. Otto, J. Guck, and S. Aland, Numerical simulation of real-time deformability cytometry to extract cell mechanical properties, ACS Biomater. Sci. Eng. **3**, 2962 (2017).
[23] S. Girardo, N. Traeber, K. Wagner, G. Cojoc, C. Herold, R. Goswami, R. Schluessler, S. Abuhattum, A. Taubenberger, F. Reichel *et al.*, Standardized microgel beads as elastic cell mechanical probes, J. Mater. Chem. B **6**, 6245 (2018).
[24] M. M. Villone, J. K. Nunes, Y. Li, H. A. Stone, and P. L. Maffettone, Design of a microfluidic device for the measurement of the elastic modulus of deformable particles, Soft Matter **15**, 880 (2019).
[25] M. M. Villone and P. L. Maffettone, Dynamics, rheology, and applications of elastic deformable particle suspensions: A review, Rheol. Acta **58**, 109 (2019).
[26] B. Vonnegut, Rotating bubble method for the determination of surface and interfacial tensions, Rev. Sci. Instrum. **13**, 6 (1942).
[27] A. M. Kloxin, C. J. Kloxin, C. N. Bowman, and K. S. Anseth, Mechanical properties of cellularly responsive hydrogels and their experimental determination, Adv. Mater. **22**, 3484 (2010).
[28] T. Murata, Deformation of an elastic particle suspended in an arbitrary flow field, J. Phys. Soc. Jpn. **50**, 1009 (1981).
[29] H. A. Stone and J. W. M. Bush, Time-dependent drop deformation in a rotating high viscosity fluid, Q. Appl. Math. **54**, 551 (1996).
[30] T. Gao and H. H. Hu, Deformation of elastic particles in viscous shear flow, J. Comput. Phys. **228**, 2132 (2009).

[31] M. M. Villone, M. A. Hulsen, P. D. Anderson, and P. L. Maffettone, Simulations of deformable systems in fluids under shear flow using an arbitrary lagrangian eulerian technique, Comput. Fluids **90**, 88 (2014).
[32] H. H. Hu, N. A. Patankar, and M. Y. Zhu, Direct numerical simulations of fluid–solid systems using the arbitrary Lagrangian–Eulerian technique, J. Comput. Phys. **169**, 427 (2001).
[33] R. von Mises, Mechanik der festen Körper im plastisch-deformablen Zustand, Nachrichten von der gesellschaft der wissenschaften zu göttingen, Math.-Physik. Klasse **4**, 582 (1913) .
[34] H. H. Hu and D. D. Joseph, Evolution of a liquid drop in a spinning drop tensiometer, J. Colloid Interface Sci. **162**, 331 (1994).
[35] R. W. Style, C. Hyland, R. Boltyanskiy, J. S. Wettlaufer, and E. R. Dufresne, Surface tension and contact with soft elastic solids, Nat. Commun. **4**, 1 (2013).
[36] R. W. Style, R. Boltyanskiy, Y. Che, J. S. Wettlaufer, L. A. Wilen, and E. R. Dufresne, Universal Deformation of Soft Substrates Near a Contact Line and the Direct Measurement of Solid Surface Stresses, Phys. Rev. Lett. **110**, 066103 (2013).
[37] A. Carbonaro, K. N. Chagua-Encarnacion, C. Charles, T. Phou, C. Ligoure, S. Mora, and D. Truzzolillo, Spinning elastic beads: a route for simultaneous measurements of the shear modulus and the interfacial energy of soft materials, Soft Matter (2020).
[38] R. Roscoe, On the rheology of a suspension of viscoelastic spheres in a viscous liquid, J. Fluid Mech. **28**, 273 (1967).